Soft Matter

PAPER

View Article Online
View Journal | View Issue

Cite this: *Soft Matter*, 2016, 12, 4463

Surface tension regularizes the crack singularity of adhesion

Stefan Karpitschka,*[a] Leen van Wijngaarden[a] and Jacco H. Snoeijer[ab]

Received 21st December 2015,
Accepted 1st April 2016

DOI: 10.1039/c5sm03079j

www.rsc.org/softmatter

The elastic and adhesive properties of a solid surface can be quantified by indenting it with a rigid sphere. Indentation tests are classically described by the JKR-law when the solid is very stiff, while recent work highlights the importance of surface tension for exceedingly soft materials. Here we show that surface tension plays a crucial role even in stiff solids: Young's wetting angle emerges as a boundary condition and this regularizes the crack-like singularity at the edge of adhesive contacts. We find that the edge region exhibits a universal, self-similar structure that emerges from the balance of surface tension and elasticity. The similarity theory is solved analytically and provides a complete description of adhesive contacts, by which we reconcile global adhesion laws and local contact mechanics.

1 Introduction

The adhesion between two solid bodies in contact is extremely common in nature and technology.[1–4] Adhesive contacts are described by a classical law derived by Johnson, Kendall and Roberts (JKR),[5] providing the benchmark to characterize elastic and adhesive material properties.[6–8] Despite its success, JKR theory does not provide a complete description of the physics inside the contact. Namely, the elastic problem is considered without explicitly treating adhesive interactions, while furthermore the contact exhibits a crack-like elastic singularity at the edge. This issue was elegantly resolved in a macroscopic theory, where, by analogy with fracture mechanics, the elastic energy released by opening the crack is balanced by the work of adhesion.[9–13]

Recent studies on very soft gels and rubbers provided a very new perspective on adhesive contacts.[14–19] Just like fluids, these soft materials are highly susceptible to a Laplace pressure due to surface tension.[20–24] This insight exposed a profound link between "solid adhesion" and "liquid wetting":[14–19] both are adhesive contacts, but whether they are solid-like or liquid-like depends on the contact size (ℓ in Fig. 1) compared to the elastocapillary length γ/μ, the ratio of surface tension γ to shear modulus μ. Liquid-like contacts were for example found for soft gels[15] and nanoparticles.[17]

Intriguingly, the extreme case of liquid wetting ($\mu = 0$) does not suffer from the crack singularity: it is governed by a benign boundary condition in the form of Young's wetting angle. This is in stark contrast to adhesion theories at finite μ, which rely on global energy estimates[15–17] or on the energy released by displacing the crack-like elastic singularity.[18,19] Hence, despite the deep connection between wetting and adhesion, the theoretical description of elastic contacts has remained very different from that of a wetting liquid. In combination with recent experimental observations,[25] this in particular provokes the question: What happens at the edge of elastic adhesive contacts?

In this paper we provide a unifying description of adhesive contacts, including a regularisation of the crack singularity. Variational analysis provides the key insight: even at a large

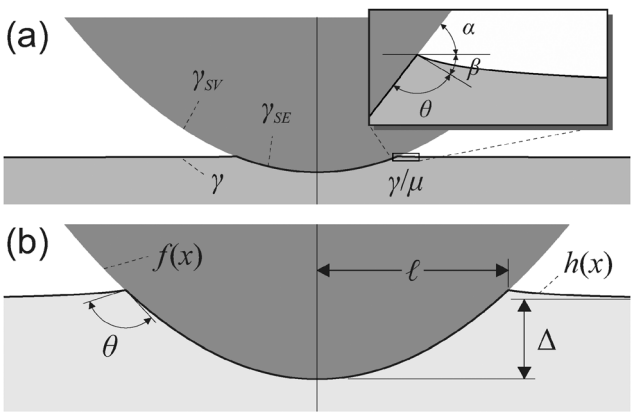

Fig. 1 Adhesive contact between an elastic layer and a rigid indenter. (a) Stiff contact, the elasto-capillary length γ/μ is much smaller than the contact size ℓ. (b) Soft contact, γ/μ is comparable to ℓ. Profiles $h(x)$ are solutions of our local two-dimensional contact theory (vertical scale stretched), $f(x)$ the shape of the indenter. The upper case is in the classical JKR regime, for which we identify a narrow, universal zone that is governed by a wetting angle θ, regularizing the crack singularity (inset).

[a] Physics of Fluids Group, Faculty of Science and Technology, Mesa+ Institute, University of Twente, 7500 AE Enschede, The Netherlands. E-mail: j.h.snoeijer@utwente.nl
[b] Mesoscopic Transport Phenomena, Eindhoven University of Technology, Den Dolech 2, 5612 AZ Eindhoven, The Netherlands

elastic modulus, adhesive contacts are governed by a wetting angle θ boundary condition [*cf.* zoom in Fig. 1(a)], as long as γ/μ remains larger than the scale of molecular interactions. In such a purely macroscopic description, we show how such a wetting angle in solid mechanics regularizes the crack singularity at a length scale γ/μ. Throughout this paper we will assume that the surface energies do not depend on the state of elastic strain, so that the surface stress is identical to the surface tension.[26] Under these conditions, the boundary condition for the wetting angle is simply given by Young's law, even for relatively large elastic moduli. Another key result is that, remarkably, the contact exhibits at the edge a self-similar structure that is captured by a single, universal similarity solution that is solved analytically. The similarity theory provides a unification of solid adhesion and liquid wetting, in which global adhesion laws and local contact mechanics are fully reconciled.

This paper is organized as follows. In Section 2 we present the variational analysis by which we formulate the adhesion problem, including the appropriate boundary conditions. This problem is then worked out explicitly in the context of linear elasticity for a cylindrical indenter in Section 3. We show numerical solutions that reveal the full details of the deformation and stress distribution inside and outside the contact. Section 4 provides a detailed analysis of the universality of the edge region, for which we derive a similarity theory. This paper closes with a discussion in Section 5.

2 Variational analysis: the wetting angle

Instead of analysing the energy released upon opening a crack,[11,13,18,19] we pose the macroscopic free energy of the problem sketched in Fig. 1, and derive a boundary condition by direct variational analysis. We assume large deformations compared to the range of molecular interactions, allowing macroscopic theory that is based on surface energies.[12] Still, one can use linear elasticity theory since displacements are typically much smaller than the size of the contact ℓ (Fig. 1). Within this framework, we show that the boundary condition is given by a wetting angle θ, satisfying Young's law based on the surface tensions. This wetting angle replaces the crack singularity, and provides a natural link between adhesion of solids and liquids.

2.1 The free energy functional

We pose the problem for a two-dimensional indenter on an infinite half space under plane strain conditions, which is generalized to the axisymmetric case in Appendix A. As soft materials are nearly incompressible, the no-slip boundary condition between the indenter and the elastic medium does not induce shear stress;[27] hence, even for frictional contacts it suffices to consider only the normal displacement $h(x)$ of the elastic layer.[19] We remark that on the two-dimensional half space, the displacement is defined only up to a constant of integration. The analysis below does not depend on the choice of the reference point, so one can use $h(x)$ as the elastic degree of freedom.

The free energy of the problem then consists of an elastic contribution, the functional $\mathscr{F}_{\rm el}[h]$ that is given explicitly in Appendix B, and capillary contributions due to the surface energies γ, $\gamma_{\rm SV}$, and $\gamma_{\rm SE}$ [*cf.* Fig. 1(a)]. The work of adhesion $W = \gamma + \gamma_{\rm SV} - \gamma_{\rm SE}$ represents the reduction in the surface energy when brought into contact. Minimization of $\mathscr{F}_{\rm el}[h]$ is constrained, since the elastic surface must comply with the shape of the indenter $f(x)$. This gives the constraint $h(x) = f(x) + \Delta$ over the range $-\ell \le x \le \ell$, where $-\Delta$ is the distance by which the solid is indented defined with respect to some arbitrary reference point. Taking also into account the work done by the external load $f_{\rm 2D}$, the relevant functional is,

$$\begin{aligned}\mathscr{F}[h(x);\ell,\Delta] &= \mathscr{F}_{\rm el}[h(x)] + \int_\ell^\infty \mathrm{d}x\,\gamma\left(1+h'^2\right)^{1/2} \\ &\quad + \int_\ell^\infty \mathrm{d}x\,\gamma_{\rm SV}\left(1+f'^2\right)^{1/2} + \int_0^\ell \mathrm{d}x\,\gamma_{\rm SE}\left(1+f'^2\right)^{1/2} \\ &\quad + \int_0^\ell \mathrm{d}x\,p(x)\{h(x) - [f(x)+\Delta]\} \\ &\quad + \lambda\{h_+(\ell) - [f(\ell)+\Delta]\} + \frac{1}{2}f_{\rm 2D}\Delta,\end{aligned} \tag{1}$$

where we used the symmetry $x \to -x$, so that $\mathscr{F}$ is half the total energy. The integrals in the upper line give the surface areas multiplied by their interfacial energies. Importantly, we implicitly assumed here that the surface energies do not depend on the elastic strain, so we do not distinguish between surface energy and surface stress.[26,28–30] Releasing this condition would require more elastic degrees of freedom than only $h(x)$. Compliance in the contact zone is imposed by the continuous Lagrange multiplier $p(x)$. Without imposing the slope outside the contact, we require $h(x)$ to be continuous at $x = \ell$, here enforced by the Lagrange multiplier λ [$h_+(\ell) = \lim_{x\to\ell^+} h(x)$]. We remark that the resulting variational problem resembles that of a liquid drop on an elastic layer.[31]

2.2 Equilibrium conditions by variation

The degrees of freedom of the problem are $h(x)$, ℓ, Δ, which should minimize the functional (1). The variation of Δ is given by a simple partial derivative

$$\frac{\partial\mathscr{F}}{\partial\Delta} = 0 = \frac{1}{2}f_{\rm 2D} - \lambda - \int_0^\ell \mathrm{d}x\,p(x). \tag{2}$$

Next we perform the variation $\delta h(x)$,

$$\begin{aligned}\delta\mathscr{F} &= 0 = \left[\lambda - \frac{\gamma h'}{(1+h'^2)^{1/2}}\right]_{\ell_+}\delta h(\ell_+) + \int_0^\ell \mathrm{d}x\,\delta h(x)[\sigma(x)+p(x)] \\ &\quad + \int_\ell^\infty \mathrm{d}x\,\delta h(x)\left[\sigma(x) - \frac{\gamma h''}{(1+h'^2)^{3/2}}\right],\end{aligned} \tag{3}$$

where the second boundary term appears through the usual integration by parts. We also used $\sigma \equiv \delta\mathscr{F}_{\rm el}/\delta h$ as the elastic normal stress,[32] see also Appendix B. At $x = \ell_+$ this implies

$$\lambda = \gamma\left[\frac{h'}{(1+h'^2)^{1/2}}\right]_{\ell_+} = -\gamma\sin\beta, \tag{4}$$

where β is the (downward) angle with respect to the horizontal – see the inset of Fig. 1a. Using this equation to eliminate λ combined with (2) gives

$$f_{2D} = -2\gamma \sin\beta - \int_{-\ell}^{\ell} \mathrm{d}x\, \sigma(x), \tag{5}$$

where we used that $p(x) = -\sigma(x)$ inside the contact. The integrals in (3) separate into the domains inside the contact, where indeed $\sigma(x) = -p(x)$, while outside

$$\sigma = \frac{\gamma h''}{(1+h'^2)^{3/2}}, \quad |x| > \ell, \tag{6}$$

In line with ref. 20–24, the latter equilibrium condition expresses that the elastic stress outside the contact does not vanish, but is given by the solid Laplace pressure.

Finally, we perform the variation of ℓ:

$$\frac{\partial \mathscr{F}}{\partial \ell} = 0 = -\gamma\left(1+h_+'^2\right)^{1/2} + (\gamma_{SE}-\gamma_{SV})\left(1+f'^2\right)^{1/2} + \lambda h_+{}' - \lambda f', \tag{7}$$

where derivatives h' are to be evaluated at $x = \ell_+$. Substituting λ from (4) gives

$$\gamma\left[\frac{1}{(1+h_+'^2)^{1/2}}\frac{1}{(1+f'^2)^{1/2}} + \frac{h_+{}'}{(1+h_+'^2)^{1/2}}\frac{f'}{(1+f'^2)^{1/2}}\right] = \gamma_{SE} - \gamma_{SV}. \tag{8}$$

Introducing now the angle of the solid with respect to the horizontal α (inset of Fig. 1a), one recognizes

$$\gamma[\cos\alpha\cos\beta - \sin\alpha\sin\beta] = \gamma\cos(\alpha+\beta) = -\gamma\cos\theta = \gamma_{SE} - \gamma_{SV}. \tag{9}$$

This is the solid analogue of Young's law, which serves as a boundary condition at $x = \ell$.

2.3 Summary: the adhesion problem

Let us briefly summarize the adhesion problem that emerges from the variational analysis:

$$h(x) = f(x) + \Delta, \quad |x| < \ell, \tag{10}$$

$$\sigma(x) = \frac{\gamma h''}{(1+h'^2)^{3/2}}, \quad |x| > \ell, \tag{11}$$

$$\gamma\cos\theta = \gamma_{SV} - \gamma_{SE}, \quad x = \pm\ell, \tag{12}$$

The first equation reflects the compliance inside the contact. The second equation holds outside the contact and expresses the balance of elastic stress and the Laplace pressure due to the surface tension of the solid. The three-dimensional axisymmetric variational analysis gives similar equilibrium conditions, except that eqn (11) contains an extra azimuthal curvature contribution. The third equation is simply Young's law, familiar for wetting problems but here derived for an elastic layer. Finally, the total force reads

$$f_{2D} = -2\gamma \sin\beta - \int_{-\ell}^{\ell} \mathrm{d}x\, \sigma(x), \tag{13}$$

with the equivalent expression for the axisymmetric case

$$f_{3D} = -2\pi\ell\gamma \sin\beta - \int_0^{\ell} \mathrm{d}r 2\pi r\sigma(r). \tag{14}$$

The crux of the analysis is the appearance of Young's wetting angle θ, defined in Fig. 1: it serves as the boundary condition emerging from the variation of ℓ (also for axisymmetric contacts, *cf.* Appendix). Like in elastic wetting,[21,23,31] surface tension thus dominates over elasticity at the contact line and replaces the crack by a "wedge" geometry. In the context of solid adhesion, this is the first time that Young's angle has been derived as a boundary condition in the presence of elasticity. Previous theories derived a wetting boundary condition only in the liquid-wetting limit of vanishing elasticity.[15–17] A wetting-like boundary condition at finite elasticity was also hypothesized by Jensen *et al.*,[25] who experimentally found that a gel layer approaches the indenter at a well-defined angle that is independent of the global geometry. Apart from a first-principles explanation of this observation, the key contribution of the present analysis is that it shows that the boundary condition encodes all adhesive properties: (12) can be expressed as $W = \gamma(1 + \cos\theta)$, and the boundary condition completes the contact mechanics problem.

3 Cylindrical indenter

The system of equations eqn (10)–(13) does not require any additional minimisation step involving the energy release-rate. It forms a fully local contact mechanics problem, which in principle allows for the determination of stress over the entire contact – including the edge region. In this section we formulate the adhesion problem explicitly for a two-dimensional cylindrical indenter using linear elasticity. It is shown that the introduction of the work of adhesion through Young's contact angle indeed provides a complete description of the adhesive contact: we recover previous results in the literature, and for the first time reveal the distribution of stress inside the contact.

3.1 Formulation within linear elasticity

Within linear elasticity, the stress and displacement of the free surface of an incompressible thick layer relate as,[27]

$$\sigma(x) = -\frac{2\mu}{\pi}\int_{-\infty}^{\infty} \mathrm{d}t \frac{h'(t)}{t-x}, \tag{15}$$

with details given in the Appendix. We now focus on a cylindrical indenter of radius R, with $f(x) = \dfrac{x^2}{2R}$. The strict validity of linear elasticity requires small strains, *i.e.* $h'^2 \ll 1$, and thus θ is close to π. This simplifies the boundary condition to $h_-{}' - h_+{}' = (2W/\gamma)^{1/2}$, showing that W enters in the form a slope discontinuity.

It is advantageous to introduce dimensionless variables:

$$X = x/\ell, \quad H = hR/\ell^2, \quad F_{2D} = \frac{f_{2D}R}{\pi\mu\ell^2}, \tag{16}$$

where the external load was scaled by the result for nonadhesive (Hertz) contacts. The dimensionless parameters are

$$S = \frac{\pi\gamma}{2\mu\ell}, \quad A = \left(\frac{2WR^2}{\gamma\ell^2}\right)^{1/2}. \tag{17}$$

S represents the influence of surface tension, comparing the elasto-capillary length γ/μ to the width ℓ of the contact. A represents the work of adhesion, dictating the wetting angle. Following ref. 19 we note that outside the contact $\sigma(x) = \gamma h''(x)$, and one can further reduce (15) by integrating over the central part of the contact where the shape is known, $h' = x/R$. In dimensionless units this gives

$$SH''(X) = -\int_1^\infty \mathrm{d}T \frac{2TH'(T)}{T^2 - X^2} - \left[2 + X\ \ln\left|\frac{X-1}{X+1}\right|\right], \tag{18}$$

valid for $X > 1$, outside the contact. Here we also used the symmetry $X \to -X$ to express the integral from $-\infty\cdots-1$ in terms of the integral from $1\cdots\infty$. The slope discontinuity due to adhesion now appears as a boundary condition

$$H'(1) = 1 - A. \tag{19}$$

The integral eqn (18) with (19) completely defines the adhesive contact problem. Surface tension appears through S, while adhesion is contained in A. The examples in Fig. 1 are actual numerical profiles with $S \neq 0$, which are for the first time derived in a continuum framework.

Importantly, the boundary condition cannot be imposed without surface tension: for $S = 0$, the analysis reduces to the (two-dimensional) JKR-problem, for which we recover the crack singularity that displays a diverging slope at the edge,

$$H_0'(X) \simeq X - K(X-1)^{-1/2}. \tag{20}$$

Here K is essentially the (scaled) stress intensity factor, which reads $K = (1 - F_{2D})/2^{3/2}$ for the cylinder.[27] The inability to satisfy the boundary condition for $S = 0$ makes it a singular limit of the adhesion problem. Indeed, removing the term $SH''(X)$ in (18) changes the order of the integral equation, which comes at the expense of sacrificing a boundary condition. As is generic in such a situation, we expect the limit $S \ll 1$ to give rise to a thin boundary layer where the solution is fundamentally different from the $S = 0$ solution. Indeed, at small distances from the edge, the effect of surface tension will turn out to give a dramatic departure from the crack singularity of (20).

3.2 Numerical results for vanishing load

To illustrate that our local theory provides a complete description, we present numerical solutions to (18) with boundary condition $H'(1) = 1 - A$. Here we focus on the case of vanishing load, $f_{2D} = 0$. Without the resultant external load, the two-dimensional problem does not suffer from the problem of the reference point: the solution $h(\pm\infty) \to 0$, so that both $h(x)$ and Δ are properly defined.

3.2.1 Geometry of the adhesive contact. Fig. 2 shows how the width ℓ varies with surface tension γ [both scaled according to A and S, *cf.* (17)]. For small S we perfectly recover the result for "solid adhesion",[11,13] which in the present notation reads

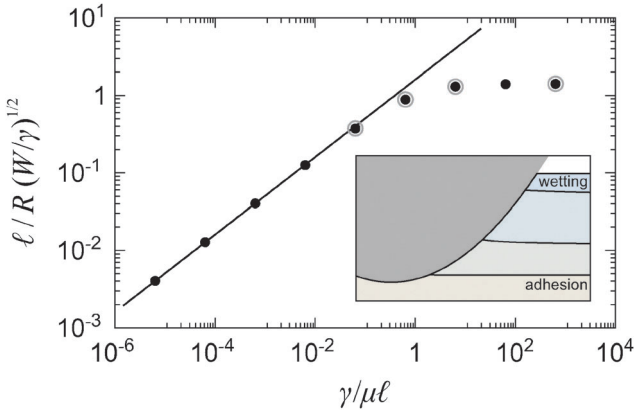

Fig. 2 Numerical solutions to the local contact mechanics eqn (18) without an external load ($f_{2D} = 0$). The contact width ℓ (made dimensionless using the scaling of A) is shown as a function of the surface tension γ (made dimensionless using the scaling of S). For small $\gamma/\mu\ell$, we recover the JKR scaling [solid line, (21)], while for large $\gamma/\mu\ell$ the width saturates. The inset shows the corresponding profiles $h(x)$ for $S = 10^{-1}$, 1, 10, 10^3 (grey circles in the main plot).

$$\ell = \left(\frac{8R^2W}{\pi\mu}\right)^{1/3} \Rightarrow AS^{1/2} = 2^{-3/2}\pi. \tag{21}$$

This is the two-dimensional equivalent of the JKR law, and is shown as the solid line in Fig. 2. The fact that this classical result is recovered, without considering the energy release rate, confirms that Young's contact angle provides the correct boundary condition at the edge of the contact. It is interesting to also consider the regime of large surface tension (or vanishing μ), for which the contact width becomes independent of S. The numerical results in Fig. 2 saturate to the value expected for "liquid wetting". This agrees with previous analysis and experiment,[15,17,19] but for the first time derived from an analysis of the entire contact – including the crack region.

The inset of Fig. 2 shows the numerical profiles of the elastic layer. For clarity we shifted the elastic layer rather than the rigid indenter. Clearly, the indentation $\Delta = h(0) - h(\infty)$ increases as the layer gets softer. This is further quantified in Fig. 3, showing the indentation depth $|\Delta|$ (scaled by the vertical scale ℓ^2/R) as a function of $\gamma/\mu\ell$. One again distinguishes two regimes with a crossover around $S \sim 1$, quantifying the importance of surface tension. As seen in the inset of Fig. 2, the large S limit corresponds to the case where the substrate acts like a wetting liquid, with a flat interface. In this case, the height at the edge of the contact $h(\ell) = 0$, which according to (10) requires $\Delta = -f(\ell) = -\frac{1}{2}\ell^2/R$. In the opposite limit of small S, the indentation can be computed from the $S = 0$ solution,[19,27] which amounts to $\Delta = -\frac{1}{4}\ell^2/R$.

3.2.2 Stress state of the adhesive contact. The present theory has the additional merit that it reveals the stresses near the contact edge, previously unknown due to the crack singularity. The inset of Fig. 4 shows a stress profile on the

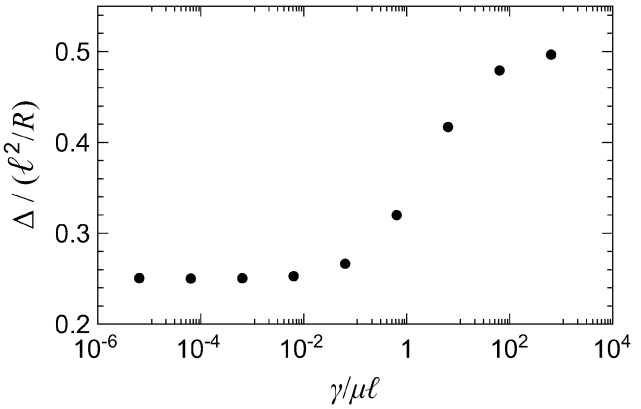

Fig. 3 The same solutions as in Fig. 2, now showing the indentation depth $|\Delta|$ (scaled by ℓ^2/R) as a function of the dimensionless surface tension $\gamma/\mu\ell$. The asymptotes for small and large surface tensions, respectively, are $|\Delta|R/\ell^2$ = 1/4 and 1/2 (see the text).

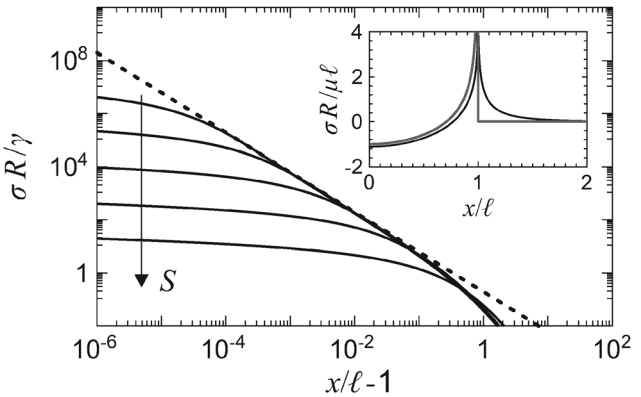

Fig. 4 Stress profiles σ outside the contact with f_{2D} = 0, for $S = 10^{-4}, 10^{-3}, 10^{-2}, 10^{-1}, 1$. The stress exhibits a $-3/2$ scaling (dashed line), regularized by a logarithmic zone as $x \to \ell$. Inset: Stress profile on the scale of the contact. The grey line is the JKR profile (S = 0) and the black line is the typical profile with surface tension (S = 1).

scale of the contact (S = 1, black line). The stress extends both inside and outside the contact and exhibits a weak, logarithmic singularity. As is generic for elastic free surfaces with a slope-discontinuity,[33] the stress diverges as $\sigma \sim \mu \log|X-1|$, with a strength proportional to that of the discontinuity.† This is very different from the JKR theory (S = 0), which has the square root singularity at the inside and vanishing stress outside the contact (inset, grey line). The main panel in Fig. 4 shows details of the stress when approaching $x \to \ell$ from the outside of the contact. Different curves correspond to different S values. One observes the appearance of a $-3/2$ power law for the stress at a large distance from the contact, which is logarithmically smoothened at small distances where surface tension becomes dominant.

† The logarithmic stress divergence due to a small discontinuity in h' lies within the realm of linear elasticity.[33] The scaling (27) confirms that $\sigma \sim \mu$ only within an asymptotically small region near the contact, $X - 1 < S\exp\left(-\sqrt{\gamma/W}\right)$, where we note that the present analysis assumes $(W/\gamma)^{1/2} \ll 1$.

As anticipated, the smoothening range near the edge acts like a boundary layer to the large scale profile, necessary to accommodate the wetting angle θ. The cross-over observed in Fig. 2, reporting global features of the contact, can thus be explained from the physics inside the contact: the transition from "adhesion" to "wetting" appears when the influence of surface tension, the smoothing zone, becomes comparable to the size of the contact, *i.e.* $\gamma/\mu \sim \ell$.

4 Universality of the edge region

We now turn our attention to the edge of the contact, focussing on the case of small surface tension $S \ll 1$. In this section we analyse the edge of the contact by a boundary layer analysis. We expose the self-similar nature of the edge region, derive an analytical solution to the boundary layer, and show how the classical JKR law emerges from a matched asymptotic expansion.

4.1 Similarity solution

Since the extent of surface tension is bound to a thin region that scales with S, we propose the similarity form,

$$H'(X) = X + A\mathscr{H}'(\zeta), \quad \zeta = \frac{X-1}{S}, \tag{22}$$

valid for $S \ll 1$. Here $\mathscr{H}(\zeta)$ is a universal function that inside the boundary layer replaces, and as such regularizes, the crack singularity in (20). One verifies that the boundary condition $H'(1) = 1 - A$ reads $\mathscr{H}'(0) = -1$ in terms of the similarity function.

It is possible to obtain a closed equation for $\mathscr{H}(\zeta)$. However, one cannot directly insert (22) into (18), since the similarity Ansatz is only valid inside the boundary layer. Outside the boundary layer we expect to recover the solutions for S = 0, denoted as $H_0(X)$, which are superpositions of the usual (2D) Hertz and punch solutions.[5,27] We therefore treat (18) by spliting the domain of integration into two parts:

$$\begin{aligned} SH''(X) \;=\; & -\int_1^{1+S^{1/2}} \mathrm{d}T \frac{2TH'(T)}{T^2-X^2} - \int_{1+S^{1/2}}^{\infty} \mathrm{d}T \frac{2TH'(T)}{T^2-X^2} \\ & - \left[2 + X\ln\left|\frac{X-1}{X+1}\right|\right], \quad X > 1. \end{aligned} \tag{23}$$

The scale $S^{1/2}$ is intended as an intermediate length scale between the boundary layer thickness S and the scale of the contact: for small S, it gives the hierarchy of scales $S \ll S^{1/2} \ll 1$. This implies that the first integral in (23) is a full integral over the boundary layer, while the second integral is strictly outside the boundary layer where $H(T) \simeq H_0'(T)$. Since $H_0'(T)$ satisfies (18) with S = 0, we infer for asymptotically small S,

$$-\int_{1+S^{1/2}}^{\infty} \mathrm{d}T \frac{2TH'(T)}{T^2-X^2} - \left[2 + X\ln\left|\frac{X-1}{X+1}\right|\right] \simeq 0. \tag{24}$$

Hence, (23) reduces to

$$SH''(X) = -\int_1^{1+S^{1/2}} \mathrm{d}T \frac{2TH'(T)}{T^2-X^2}, \quad X > 1. \tag{25}$$

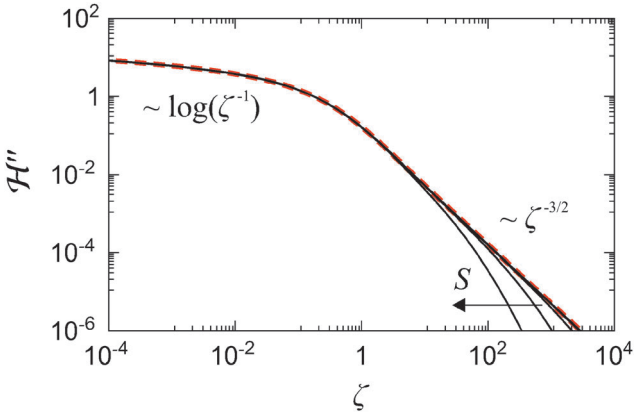

Fig. 5 The similarity function $\mathscr{H}''(\zeta)$ describing the crack region (red, dashed). Superimposed are the stress profiles of Fig. 4, scaled according to (27), confirming the self-similarity.

The final step is to insert the similarity form (22), introduce $X = 1 + S\zeta$ and $T = 1 + S\zeta'$, and evaluate the terms in orders of S. The leading order $\sim S^0$, and gives

$$\mathscr{H}''(\zeta) = -\int_0^\infty \mathrm{d}\zeta' \frac{\mathscr{H}'(\zeta')}{\zeta' - \zeta}. \tag{26}$$

Complemented by the boundary condition $\mathscr{H}'(0) = -1$, this fully determines the similarity function.

The numerical solution to (26) is represented in Fig. 5, showing $\mathscr{H}''(\zeta)$ as the red dashed line. Owing to the capillary stress relation, $\sigma = \gamma h'' = \gamma A \mathscr{H}''/RS$ (valid for small slopes), the similarity Ansatz in fact predicts a collapse of all stress profiles:

$$\sigma(x) = \frac{2^{3/2}\mu}{\pi}\left(\frac{W}{\gamma}\right)^{1/2} \mathscr{H}''(\zeta). \tag{27}$$

Fig. 5 shows that the scaled stress profiles of Fig. 4 perfectly collapse on the predicted dashed line, illustrating the validity of the similarity theory. In particular, it confirms the emergence of a weak logarithmic singularity of the stress at the edge of the contact.

4.2 Analytical solution for $\mathscr{H}'(\zeta)$

In this paragraph we derive the analytical solution to (26). In terms of the Laplace transform of $\mathscr{H}'(\zeta)$, the solution reads

$$\mathscr{L}\{\mathscr{H}'(\zeta)\}(s) = \frac{-1}{s^{1/2}(s^2+\pi^2)^{1/4}} \exp\left(-\int_s^\infty \mathrm{d}t \frac{\ln(t/\pi)}{t^2+\pi^2}\right). \tag{28}$$

Based on this, we infer the asymptotics for $\zeta \ll 1$,

$$\mathscr{H}' \simeq -1 - \zeta \ln \zeta, \tag{29}$$

which indeed satisfies the boundary condition $\mathscr{H}'(0) = -1$. For $\zeta \gg 1$ it is found that,

$$\mathscr{H}' \simeq -\frac{1}{\pi \zeta^{1/2}}. \tag{30}$$

This result is critical to analytically derive the JKR-law. Both asymptotes are indicated in Fig. 5 where we represent $\mathscr{H}''(\zeta)$.

The solution (28) was derived by following Varley and Walker,[34] VW henceforth. VW considered singular integral equations of the form

$$u(\xi) = \frac{1}{\pi}\int_0^\infty \mathrm{d}\xi' \frac{v(\xi')}{\xi' - \xi}, \tag{31}$$

where u and v are not arbitrary functions, but restricted to

$$u(\xi) = a_1 F'(\xi) + a_0 F(\xi), \quad v(\xi) = b_1 F'(\xi) + b_0 F(\xi). \tag{32}$$

Indeed, (26) is of the type (31). This is seen by introducing $\xi = \pi\zeta$, $\mathscr{H}'(\zeta) = \pi F(\xi)$, which brings (26) to the form

$$F'(\xi) = -\frac{1}{\pi}\int_0^\infty \mathrm{d}\xi' \frac{F(\xi')}{\xi' - \xi}, \quad \text{with} \quad F(0) = -\frac{1}{\pi}. \tag{33}$$

This corresponds to (31) with $a_0 = 0$, $a_1 = 1$, $b_0 = -1$, and $b_1 = 0$.

Following VW, we define the Laplace transform of $F(\xi)$ by

$$K(p) = \mathscr{L}\{F(x)\}(p) = \int_0^\infty \mathrm{d}\xi F(\xi) \mathrm{e}^{-p\xi}. \tag{34}$$

Taking the Laplace transform of (33) reduces the integro-differential equation to the integral equation

$$\pi p K(p) + 1 - \int_0^\infty \mathrm{d}q \frac{K(q)}{q - p} = 0. \tag{35}$$

With the help of complex function theory, VW solved the corresponding equation for the general case (31), which for the present values of a_0, a_1, b_0, and b_1 reduces to

$$K(p) = -\frac{1}{\pi}\frac{1}{p^{1/2}(p^2+1)^{1/4}} \exp\left(-\frac{1}{\pi}\int_p^\infty \mathrm{d}t \frac{\ln t}{1+t^2}\right). \tag{36}$$

The solution (28) is obtained as $K\left(\frac{s}{\pi}\right)$, after returning from ξ to ζ.

The asymptotes (29) and (30) are, respectively, derived by considering the small and large p behaviour of $K(p)$. For large p,

$$\int_p^\infty \mathrm{d}t \frac{\ln t}{1+t^2} \simeq \int_p^\infty \mathrm{d}t \frac{\ln t}{t^2} = \frac{\ln p}{p} + \frac{1}{p}, \tag{37}$$

such that

$$K(p) \simeq -\frac{1}{\pi p} + \frac{\ln p}{(\pi p)^2}. \tag{38}$$

Upon inversion, and using $K\left(\frac{s}{\pi}\right)$, this gives (29). The large ζ asymptote corresponds to small p, which is governed by the branch point of $K(p)$ in $p = 0$. This reads

$$K(p) \simeq -\frac{1}{\pi p^{1/2}}. \tag{39}$$

which leads to (30).

4.3 Adhesion laws: matched asymptotics

4.3.1 Cylindrical indenter. To complete the analysis, we demonstrate how the adhesion laws are recovered. In eqn (30) we demonstrated that for large ζ, $\mathscr{H}'$ reads $\mathscr{H}' \simeq -1/(\pi\zeta^{1/2})$. This is of prime importance as it can be matched to the square root divergence of (20), which is the singular crack solution for the case $S = 0$.

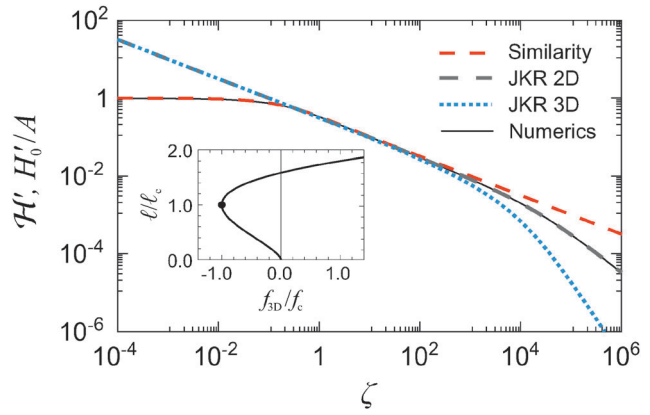

Fig. 6 Matching the asymptotes of the similarity solution $\mathscr{H}'$ (red, dashed), to the singular outer solutions H_0'/A for the cylinder (gray dashed) or sphere (blue dotted). The solid black line shows the 2D numerics: it follows H_0' on large scales, switching to $\mathscr{H}'$ on small scales. The matching was done for $S = 10^{-4}$, while the external load was set to the critical value for pull-off (inset, circle). Inset: ℓ *versus* f_{3D} given by eqn (41), scaled by the critical values f_c, ℓ_c. For a given load, the upper (lower) branch is stable (unstable).[33]

The matching is illustrated in Fig. 6: when the effect of surface tension is small, $S \ll 1$, one observes an overlap between the inner solution ($\mathscr{H}'$, red dashed) and the outer solution (H_0', gray dashed). Equating the prefactors of the asymptotes gives,

$$K = \pi^{-1} A S^{1/2} \Rightarrow 1 - \frac{f_{2D} R}{\pi \mu \ell^2} = \left(\frac{8 W R^2}{\pi \mu \ell^3}\right)^{1/2}, \qquad (40)$$

where in the second step we used the dimensionless stress intensity factor $K = (1 - F_{2D})/2^{3/2}$.

The matching condition (40) coincides with the adhesion law for the cylindrical indenter.[11,13] For the case $f_{2D} = 0$ it reduces to (21), while without adhesion it gives the Hertz law between the size of the contact ℓ and the applied load. The similarity theory gives a physical description of this result: the adhesion imposes a wetting angle at the edge of the contact, which by means of a surface tension-dominated boundary layer is connected to the elastic displacements on the much larger scale of the contact. This is further highlighted by the full numerical solution (Fig. 6, solid line), confirming that surface tension regularizes the $-1/2$ singularity.

4.3.2 Spherical indenter. Analogously, the same matching gives the JKR-law for the spherical indenter. The boundary layer is asymptotically thin compared to the contact radius, so the physics at the edge is quasi-one-dimensional (see also ref. 35). The spherical contact is therefore governed by a boundary layer of the same universal form $\mathscr{H}(\zeta)$ and again requires a matching to the singular H_0 (Fig. 6, blue dotted). Evaluating K for the spherical indenter recovers the JKR-law:[5]

$$K = \pi^{-1} A S^{1/2} \Rightarrow 1 - \frac{3 f_{3D} R}{16 \mu \ell^3} = \left(\frac{9 \pi W R^2}{8 \mu \ell^3}\right)^{1/2}, \qquad (41)$$

confirming the validity of the approach. For completeness, we illustrate this famous relation between ℓ and the load f_{3D} in the inset of Fig. 6. The outer solutions shown in the main panel actually correspond to the minimum (negative) load, which is the critical point where the indenter is pulled off from the elastic.

5 Discussion

The present analysis provides a unification of solid adhesion and liquid wetting, for the first time captured in a theory that contains the full details of the contact mechanics. The main assumptions underlying the theory are essentially equivalent to those in the classical JKR theory: reversibility of the adhesion process (*e.g.* no plasticity), and elastic deformations need to be larger than the range of molecular forces, yet small enough to allow for linear elasticity. In addition, we have assumed that the surface tension of the gel has no explicit strain-dependence. Within this context it is demonstrated that the adhesion properties are fully encoded by Young's law for the wetting angle, even at finite elasticity. This newly identified boundary condition for elastic adhesive contacts necessitates a thin boundary layer at the edge of the contact, which regularizes the JKR-crack singularity. Here we analytically resolve the boundary layer in the form of a similarity solution. The analysis is backed up by numerical solutions, by which we also recover the crossover from JKR to the surface tension dominated regime for exceedingly soft contacts.[18,19]

The emergence of a contact angle boundary condition will be a robust feature that applies beyond most of the restrictions quoted above. For example, the solution given here is restricted to linear elasticity, $(W/\gamma)^{1/2} \ll 1$, but the boundary condition (12) equally applies nonlinearly – as also suggested by recent experiments.[25] This paves the way to analyse adhesion involving large deformations. In this context, an important aspect for future studies is a systematic derivation of the boundary condition whenever the surface energy depends on the strain.[15,26,28–30] Also the concept of hysteresis, *i.e.* the difference in the work of adhesion during loading and unloading,[36,37] might have a counterpart in terms of contact angles: in liquid wetting this is described by contact angle hysteresis. It would be interesting to see if adhesion can also be captured by an advancing and receding contact angle. Another noteworthy aspect is that at very small contact angles (close to complete wetting), the solvent can be separated from the gel in the vicinity of the edge,[25] also observed in simulations of microgel particles.[38] We do note that the concept of "wetting angles" must break down for contacts that are sufficiently stiff such that elastic deformations fall within the range of molecular interactions,[12] *i.e.* when approaching the DMT regime.

In a broader context, we hypothesize that the self-similarity derived here for adhesive contacts could be a generic feature of instabilities and fracture in the presence of surface tension,[39–41] as is the case for fracture of viscous liquids.[42,43]

A Variational analysis of the spherical indenter

The variational formulation of the adhesive contact problem can be straightforwardly extended to axisymmetric indenters of

shape $f(r)$. The free energy is similar as in 2D, but contains extra factors $2\pi r$ since the integrals now represent axisymmetric areas:

$$\begin{aligned}\mathscr{F}[h(r);\ell,\Delta] &= \mathscr{F}_{\mathrm{el}}[h(r)] + \int_{\ell}^{\infty} \mathrm{d}r 2\pi r\gamma \left(1+h'^2\right)^{1/2} \\ &+ \int_{\ell}^{\infty} \mathrm{d}r 2\pi r\gamma_{\mathrm{SV}} \left(1+f'^2\right)^{1/2} \\ &+ \int_{0}^{\ell} \mathrm{d}r 2\pi r\gamma_{\mathrm{SE}} \left(1+f'^2\right)^{1/2} \\ &+ \int_{0}^{\ell} \mathrm{d}r 2\pi r p(r)\{h(r)-[f(r)+\Delta]\} \\ &+ \lambda\{h(\ell_+)-[f(\ell)+\Delta]\} + f_{3\mathrm{D}}\Delta.\end{aligned} \tag{42}$$

For convenience (and without the loss of generality), we defined the continuous Lagrange multiplier to be $2\pi r p(r)$. This has the merit that, as in the 2D case, $p(r)$ can be interpreted as the contact pressure.

The degrees of freedom of the problem are $h(r)$, ℓ, Δ. The variation of Δ gives

$$\frac{\partial \mathscr{F}}{\partial \Delta} = 0 = f_{3\mathrm{D}} - \lambda - \int_0^{\ell} \mathrm{d}r 2\pi r p(r). \tag{43}$$

Next we perform the variation $\delta h(r)$,

$$\begin{aligned}\delta\mathscr{F} = 0 = &\left[\lambda - 2\pi r \frac{\gamma h'}{\left(1+h'^2\right)^{1/2}}\right]_{\ell_+} \delta h(\ell_+) + \int_0^{\ell} \mathrm{d}r 2\pi r \delta h(r)[\sigma(r)+p(r)] \\ &+ \int_{\ell}^{\infty} \mathrm{d}r 2\pi r \delta h(r)\left[\sigma(r) - \gamma\left(\frac{h''}{\left(1+h'^2\right)^{3/2}} + \frac{h'}{r\left(1+h'^2\right)^{1/2}}\right)\right].\end{aligned}$$

With respect to the 2D analysis, this gives a modified λ, containing a factor $2\pi\ell$:

$$\lambda = 2\pi\ell\gamma \left[\frac{h'}{\left(1+h'^2\right)^{1/2}}\right]_{\ell_+} = -2\pi\ell\gamma \sin\beta, \tag{44}$$

Another difference appears in the elastic stress outside the contact, which now becomes

$$\sigma(r) = \frac{\gamma h''}{\left(1+h'^2\right)^{3/2}} + \frac{\gamma h'}{r\left(1+h'^2\right)^{1/2}}, \quad |r| > \ell, \tag{45}$$

and contains the usual extra curvature term due to the axisymmetry. Again, we close by varying ℓ:

$$\begin{aligned}\frac{\partial \mathscr{F}}{\partial \ell} = 0 = &-2\pi\ell\gamma\left(1+{h_+}'^2\right)^{1/2} + 2\pi\ell(\gamma_{\mathrm{SE}}-\gamma_{\mathrm{SV}})\left(1+f'^2\right)^{1/2} \\ &+ \lambda {h_+}' - \lambda f'.\end{aligned}$$

Noting that λ differs from the 2D case by a factor $2\pi\ell$, the equation reduces that of the cylindrical indenter (7): also for axisymmetric indenters, Young's law emerges as the boundary condition.

B The elastic energy functional

The change in elastic free energy $\delta\mathscr{F}_{\mathrm{el}}$ can be related to the work done by the tractions acting on the boundary. In the case of a purely normal displacement $\delta h(x)$ of a two-dimensional half-space, this becomes:[32]

$$\delta\mathscr{F}_{\mathrm{el}} = \int_{-\infty}^{\infty} \mathrm{d}x\, \sigma(x)\delta h(x), \tag{46}$$

where $\sigma(x)$ is the normal stress. By definition of a functional derivative, eqn (46) expresses that $\sigma \equiv \delta\mathscr{F}_{\mathrm{el}}/\delta h$. Making use of linearity $\sigma \sim h$, (46) can be integrated to

$$\mathscr{F}_{\mathrm{el}} = \frac{1}{2}\int_{-\infty}^{\infty} \mathrm{d}x\, \sigma(x)h(x). \tag{47}$$

It is important to note that a change in the reference value for the height, *i.e.* $h(x) \to h(x) + a$, gives a finite, but constant change in the elastic free energy. This constant vanishes when the resultant loading is zero, but even at finite loading the reference value of the energy does not enter the variational analysis.

An explicit expression for the elastic energy functional is obtained using (15), so that

$$\mathscr{F}_{\mathrm{el}}[h] = \frac{\mu}{\pi}\int_{-\infty}^{\infty}\int_{-\infty}^{\infty} \mathrm{d}x\, \mathrm{d}t \frac{h(x)h'(t)}{x-t}, \tag{48}$$

which can be symmetrized by integration by parts:

$$\mathscr{F}_{\mathrm{el}}[h] = -\frac{\mu}{\pi}\int_{-\infty}^{\infty}\int_{-\infty}^{\infty} \mathrm{d}x\, \mathrm{d}t \ln|x-t| h'(x)h'(t). \tag{49}$$

Acknowledgements

We thank B. Andreotti, C.-Y. Hui, E. Raphael, T. Salez and S. K. Wilson for discussions. SK acknowledges financial support from NWO through VIDI Grant No. 11304. JS acknowledges financial support from ERC (the European Research Council) Consolidator Grant No. 616918.

References

1 B. Luan and M. O. Robbins, *Nature*, 2005, **435**, 929–932.
2 Y. Tian, N. Pesika, H. Zeng, K. Rosenberg, B. Zhao, P. McGuiggan, K. Autumn and J. Israelachvili, *Proc. Natl. Acad. Sci. U. S. A.*, 2006, **103**, 19320–19325.
3 K. V. Christ, K. B. Williamson, K. S. Masters and K. T. Turner, *Biomed. Microdevices*, 2010, **12**, 443–455.
4 C. Zhong, T. Gurry, A. A. Cheng, J. Downey, Z. Deng, C. M. Stultz and T. K. Lu, *Nat. Nanotechnol.*, 2014, **9**, 858–866.
5 K. L. Johnson, K. Kendall and A. D. Roberts, *Proc. R. Soc. London, Ser. A*, 1971, **324**, 301–313.
6 M. Chaudhury and G. Whitesides, *Langmuir*, 1991, **7**, 1013–1025.
7 Y.-S. Chu, S. Dufour, J. P. Thiery, E. Perez and F. Pincet, *Phys. Rev. Lett.*, 2005, **94**, 028102.
8 D. Pussak, D. Ponader, S. Mosca, S. V. Ruiz, L. Hartmann and S. Schmidt, *Angew. Chem.*, 2013, **52**, 6084–6087.

9 D. Maugis and M. Barquins, *J. Phys. D: Appl. Phys.*, 1978, **11**, 1989.
10 J. Greenwood and K. Johnson, *Philos. Mag.*, 1981, **43**, 697–711.
11 M. Barquins, *J. Adhes.*, 1988, **26**, 1–12.
12 D. Maugis, *J. Colloid Interface Sci.*, 1992, **150**, 243–269.
13 M. Chaudhury, T. Weaver, C. Hui and E. Kramer, *J. Appl. Phys.*, 1996, **80**, 30–37.
14 J. M. Long, G. F. Wang, X. Q. Feng and S. W. Yu, *Int. J. Solids Struct.*, 2012, **49**, 1588–1594.
15 R. W. Style, C. Hyland, R. Boltyanskiy, J. S. Wettlaufer and E. R. Dufresne, *Nat. Commun.*, 2013, **4**, 2728.
16 T. Salez, M. Benzaquen and E. Raphael, *Soft Matter*, 2013, **9**, 10699–10704.
17 Z. Cao, M. J. Stevens and A. V. Dobrynin, *Macromolecules*, 2014, **47**, 3203–3209.
18 C.-Y. Hui, T. Liu, T. Salez, E. Raphael and A. Jagota, *Proc. R. Soc. A*, 2015, **471**, 20140727.
19 T. Liu, A. Jagota and C.-Y. Hui, *Soft Matter*, 2015, **11**, 3844–3851.
20 S. Mora, T. Phou, J.-M. Fromental, L. M. Pismen and Y. Pomeau, *Phys. Rev. Lett.*, 2010, **105**, 214301.
21 E. R. Jerison, Y. Xu, L. A. Wilen and E. R. Dufresne, *Phys. Rev. Lett.*, 2011, **106**, 186103.
22 A. Marchand, S. Das, J. H. Snoeijer and B. Andreotti, *Phys. Rev. Lett.*, 2012, **108**, 094301.
23 L. Limat, *Eur. Phys. J. E: Soft Matter Biol. Phys.*, 2012, **35**, 134.
24 D. Paretkar, X. Xu, C.-Y. Hui and A. Jagota, *Soft Matter*, 2014, **10**, 4084–4090.
25 K. Jensen, R. Sarfati, R. Style, R. Boltyanskiy, A. Chakrabarti, M. Chaudhury and E. Dufresne, *Proc. Natl. Acad. Sci. U. S. A.*, 2015, **112**, 14490–14494.
26 R. Shuttleworth, *Proc. Phys. Soc., London, Sect. A*, 1950, **63**, 444–457.
27 N. I. Muskhelishvili, *Some Basic Problems of the Mathematical Theory of Elasticity*, Noordhoff, Leiden, Netherlands, 1977.
28 J. Weijs, B. Andreotti and J. H. Snoeijer, *Soft Matter*, 2013, **9**, 8494–8503.
29 S. Neukirch, A. Antkowiak and J.-J. Marigo, *Phys. Rev. E: Stat., Nonlinear, Soft Matter Phys.*, 2014, **89**, 012401.
30 C.-Y. Hui and A. Jagota, *Soft Matter*, 2015, **11**, 8960.
31 L. A. Lubbers, J. H. Weijs, L. Botto, S. Das, B. Andreotti and J. H. Snoeijer, *J. Fluid Mech.*, 2014, R1.
32 L. D. Landau and E. M. Lifshitz, *Theory of Elasticity*, Butterworth-Heinemann, Oxford, 3rd edn, 1986.
33 K. L. Johnson, *Contact Mechanics*, Cambridge University Press, Cambridge, UK, 1985.
34 E. Varley and J. Walker, *IMA J. Appl. Math.*, 1989, **43**, 11–45.
35 J. H. Snoeijer, J. Eggers and C. H. Venner, *Phys. Fluids*, 2013, **25**, 101705.
36 P. Silberzan, S. Perutz, E. Kramer and M. K. Chaudhury, *Langmuir*, 1994, **10**, 2466–2470.
37 S. Perutz, E. Kramer, J. Baney, C.-Y. Hui and C. Cohen, *J. Polym. Sci., Part B: Polym. Phys.*, 1998, **36**, 2129–2139.
38 H. Mehrabian, J. Harting and J. H. Snoeijer, *Soft Matter*, 2016, **12**, 1062.
39 G.-F. Wang, X.-Q. Feng, T.-J. Wang and W. Gao, *J. Appl. Mech.*, 2008, **75**, 011001.
40 T. Liu, R. Long and C.-Y. Hui, *Soft Matter*, 2014, **10**, 7723–7729.
41 M. K. Chaudhury, A. Chakrabarti and A. Ghatak, *Eur. Phys. J. E: Soft Matter Biol. Phys.*, 2015, **38**, 82.
42 J. Eggers, *Phys. Rev. Lett.*, 2001, **86**, 4290.
43 E. Lorenceau, F. Restagno and D. Quéré, *Phys. Rev. Lett.*, 2003, **90**, 184501.